Modeling Heating Curve for Gas Hydrate Dissociation in Porous Media

Christophe Dicharry,*,† Pascal Gayet,† Gérard Marion,† Alain Graciaa,† and Anatoliy N. Nesterov‡

Thermodynamique et Energétique des Fluides Complexes, UMR 5150, Université de Pau et des Pays de l'Adour, BP 1155, 64013 Pau, Cedex, France, and Institute of Earth Cryosphere, SB RAS, P.O. 1230, 625000 Tyumen, Russia

Received: January 28, 2005; In Final Form: July 6, 2005

A method for modeling the heating curve for gas hydrate dissociation in porous media at isochoric conditions (constant cell volume) is presented. This method consists of using an equation of state of the gas, the cumulative volume distribution (CVD) of the porous medium, and a van der Waals−Platteeuw-type thermodynamic model that includes a capillary term. The proposed method was tested to predict the heating curves for methane hydrate dissociation in a mesoporous silica glass for saturated conditions (liquid volume = pore volume) and for a fractional conversion of water to hydrate of 1 (100% of the available water was converted to hydrate). The shape factor (F) of the hydrate−water interface was found equal to 1, supporting a cylindrical shape for the hydrate particles during hydrate dissociation. Using $F = 1$, it has been possible to predict the heating curve for different ranges of pressure and temperature. The excellent agreement between the calculated and experimental heating curves supports the validity of our approach.

Introduction

The confinement of gas hydrates in porous media may affect their equilibrium dissociation temperatures and pressures compared to those obtained in the bulk (gas−bulk water−hydrate). If the pores are large, the equilibrium conditions are roughly the same as those of bulk hydrates.[1] If the pores are small, the capillary forces shift the equilibrium conditions to lower temperatures and higher pressures when compared with equilibrium conditions for bulk.[2] Since Handa and Stupin,[3] who were the first to examine the effect of pore size on the equilibrium conditions of methane and propane hydrates in mesoporous silica, several workers have addressed the effect of the confinement of hydrates in small pores on the equilibrium dissociation conditions.[4−16] Laboratory experiments[6,14,16] have shown that, for isochoric conditions (constant cell volume), the heating curve for hydrate dissociation in a porous medium with pores of varying sizes very often has a specific elongated S shape. This essentially reflects the cumulative volume distribution (CVD) of the porous medium, as clearly demonstrated by Anderson et al.[14]

Melnikov and Nesterov,[4,17] Henry et al.,[18] and Clarke et al.[19] modified the thermodynamic model for bulk hydrate originally developed by van der Waals and Platteeuw (vdWP) to include the effect of pore size on hydrate equilibrium conditions. Their model qualitatively fitted the experimental data measured in some porous media, but not quantitatively. One of the reasons why discrepancies between the measured and predicted dissociation conditions have been observed is that the model assumed that the porous media consisted of cylindrical pores with a single size rather than a distribution of pores, not necessarily cylindrical, with different sizes. However, most of porous media cannot be regarded as a "bundle of tubes" of unique size. Therefore, the models of hydrate equilibria in porous media should take into account both the pore size distribution (PSD) or, more specifically, the CVD, and the shape of the pores. Assuming a normal PSD for the porous media and using a shape factor of the hydrate−water interface, Klauda and Sandler[12] extended both their fugacity-based model and a vdWP-type model to include the effect of pore size and pore shape, and compared the equilibrium dissociation temperatures and pressures of methane hydrates in silica gels and natural porous environments predicted by these two models. Though their modified fugacity-based model seemed more accurate than the modified vdWP model, quite large discrepancies between the calculated and measured pressure values remained. Wilder et al.[9] used an extension of the vdWP model and proposed a method for reconstructing the pore volume distribution of the porous medium on the basis of the pressure−temperature dissociation diagram for the hydrates formed in the pores. In the present paper, we will solve the inverse problem.

The aim of the present work is to propose a method for predicting the heating curve for gas hydrate dissociation in porous media, at isochoric conditions. This method consists of using simultaneously an equation of state of the gas used to form the hydrates, the CVD of the porous medium, and a thermodynamic model. The model we used here is an extension of the vdWP model that includes a capillary term. The proposed method is then used to predict the heating curves for methane hydrates confined in pores of silica glass initially saturated with water.

Experimental Procedures

Research-grade methane supplied by Linde, with a reported purity of 99.995 mol % and deionized water produced by a purifier (Ultrapure Water System Milli-Q 185E from Millipore) were used in all experiments. Porous material, so-called

* Author to whom correspondence should be addressed. E-mail: christophe.dicharry@univ-pau.fr. Fax: + 33 5 59 40 76 95.

† UMR 5150.

‡ Institute of Earth Cryosphere.

10.1021/jp0504975 CCC: $30.25
Published on Web 08/18/2005

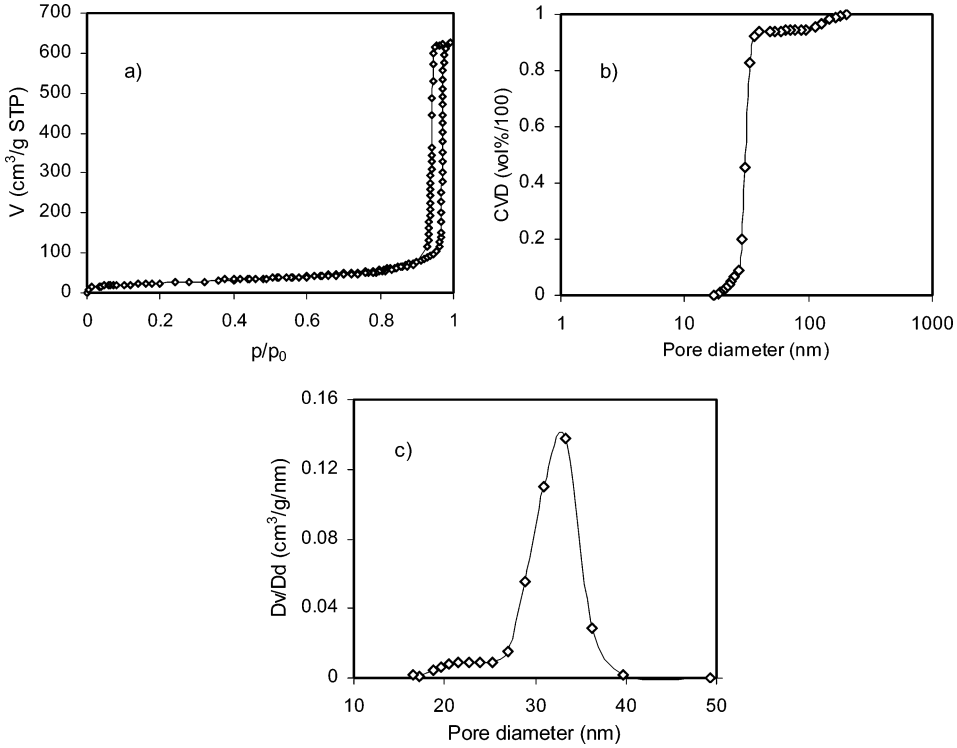

Figure 1. Characterization of the CPG sample: (a) nitrogen adsorption/desorption isotherms; (b) cumulative volume distribution (CVD); (c) pore size distribution (PSD).

TABLE 1: CPG Sample Specifications (Determined from Nitrogen Adsorption/Desorption Experiments)

property	CPG
mean mesopore diameter, d_{mean} (nm)	32
specific surface area, a_S (m^2/g)	87.8
specific mesopore volume, v_P (cm^3/g)	0.97

controlled pore glass (CPG), was purchased from CPG Inc., USA. CPG consisted of a powder of porous silica particles, with mean particle size of 37−74 μm. Nitrogen adsorption/desorption experiments were used to characterize the studied CPG sample. The sorption isotherms of nitrogen at 77 K (Figure 1a) exhibit a nearly ideal H1 type hysteresis loop, with almost vertical steps on the ascending and descending curve, which is characteristic of a mesoporous medium with a narrow PSD. The CVD and the PSD (Figure 1b and c) were computed using the Barrett−Joyner−Halenda (BJH) method,[20] applied to the desorption branch of the nitrogen isotherm. About 88% of the total pore volume was found in the pores with diameters of 25−40 nm. The specific surface area a_S was calculated using the Brunauer−Emmett−Teller (BET) model[21] using data in the 0.06−0.2 relative pressure range. The specific mesopore volume v_P was obtained from the adsorbed amount at $p/p_0 = 0.98$. The measured specifications are given in Table 1.

The $P-T$ dissociation profiles for methane hydrate formed in a CPG sample were determined using a high-pressure setup (Figure 2), which consisted of an equilibrium cell and a buffer cell both made of 316 stainless steel (maximum working pressure of 60 MPa), with a total volume of 330 cm^3 each, and a gas booster pump (Haskel AGT 32/152, maximum output pressure of about 50 MPa).

The equilibrium cell contained an extractable stainless steel socket in which the porous medium was placed for the experiments. The cells were placed in a temperature-controlled bath, whose temperature was regulated by both a heater (Julabo V/3 controlled by a Shimaden SR53) and a cooler (Huber IC045). Cell and bath temperatures were measured using PT100

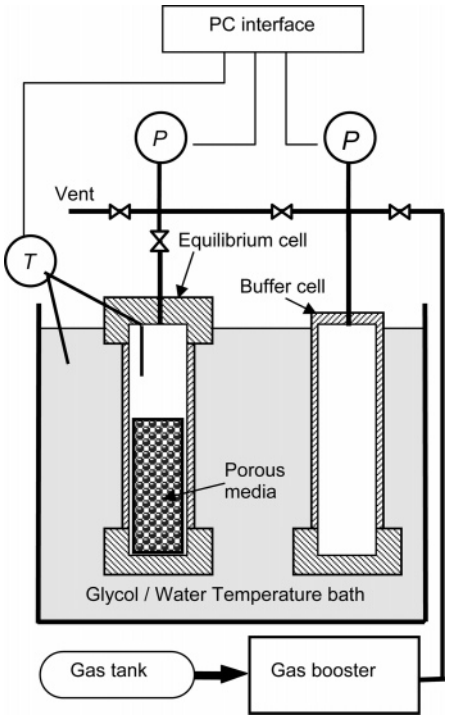

Figure 2. Schematic illustration of the experimental setup.

sensors. The PT100 sensor in the equilibrium cell was located in the gas phase between the central axis of the cell and its edge. The temperatures were measured within a precision of ±0.1 K. Cell pressures were measured with 60 MPa full-scale transducers (Keller PA-23 S transducer) calibrated with the dead-weight method to an accuracy of better than 0.02%. Bath and cell temperatures and cell pressures were continuously monitored and recorded by a computer.

The CPG sample was first dried at 383 K for at least 72 h. We verified that this temperature and this drying time were

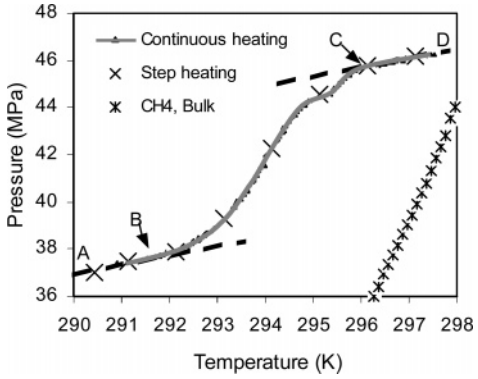

Figure 3. Experimental heating curve for gas hydrate dissociation in a porous medium.

sufficient for a CPG sample saturated with water (liquid volume = pore volume) to recover its initial weight (before water addition). However, in supplementary experiments, in which a small amount of the "dry CPG sample" was further heated to 453 K and outgassed in a vacuum microbalance (at $P = 0.4$ Pa), it was found that the sample still contained 3.05 wt % of residual adsorbed water. In the work below, this amount of residual adsorbed water will be taken into account to calculate the amount of water present in the system.

Some amount of CPG sample was then placed in the stainless steel socket, and the sample was saturated with water by adding an amount of water equal to the total pore volume. The prepared sample was placed into the equilibrium cell and kept at room temperature for at least 48 h to ensure that the pores would become completely filled with water. The cell was evacuated, and then gas methane was introduced as follows. Methane was first charged into the buffer cell from the methane cylinder via the gas booster pump to a pressure of about 50 MPa at 298 K. When the pressure in the buffer cell reached a steady-state condition, methane was allowed to divide between the buffer and equilibrium cells. Successive repetitions of this procedure made it possible to reach the desired pressure in the equilibrium cell and to calculate the number of moles of gas introduced into this cell. The gas inlet valve between the cells was then closed, and no more gas was added during the hydrate formation and dissociation procedure.

In a typical hydrate formation experiment, cell temperature was decreased to 274 K. Hydrate formation was confirmed by a steep drop in cell pressure. When cell pressure reached a steady-state condition, cell temperature was first rapidly increased to a desired temperature and then continuously increased at a rate of about 0.05 K/h. The equilibrium conditions were studied during the dissociation of hydrates because, upon heating, the equilibrium is reached more easily than upon cooling. Hydrate metastability is always present on formation, but does not occur on dissociation for a low enough heating rate. An example of heating curve for gas hydrate dissociation in a porous medium obtained by this method, known as continuous heating,[6,7] is shown in Figure 3. It should be noted that the CPG sample used in the example presented in Figure 3 was different from that used in the rest of the work. From the vendor, the mean pore diameter of this CPG sample was 12.8 nm. When the system is heated from point A, cell pressure increases with the temperature in accordance with an equation of state of the gas. The first hydrate dissociation occurs when point B is surpassed. Because smaller pore sizes require larger pressures for the hydrate to remain stable, point B will correspond to the hydrate decomposition in the smallest pores that contain hydrate. Subsequent heating leads to gradual changes in the slope of the dissociation curve. The "kink" observed in the heating curve for the temperatures between 295 and 296 K might result from a non-Gaussian-like PSD of the CPG sample used in this example. Hydrate decomposition is completed at point C, which corresponds to the hydrate dissociation in the largest pores filled with hydrate. Then further heating to point D results in a small linear pressure rise due to the expansion of the gas with the temperature. The shape of the heating curve between points B and C depends on the CVD[14] and the headspace volume (volume of the equilibrium cell occupied by free gas).[9] The location of points B and C on the heating curve depends on the amount of water converted to hydrate and the saturation state of the medium. If the fractional conversion of water to hydrate (weight of water converted to hydrate/weight of available water) is smaller than 1, the smallest pores will be filled by water not hydrate. For an undersaturated porous medium, the largest pores will be filled by gas. For a saturated medium and a fractional conversion of water to hydrate equal to 1, points B and C will correspond to the hydrate dissociation in the smallest and largest pores, respectively.

We have also reported in Figure 3 the hydrate equilibrium data obtained for the same CPG sample by a method known as step heating.[22] In these experiments, temperature was raised back to initial conditions in 1 K steps. Following each temperature rise, at least 48 h was given to the system to reach equilibrium. Figure 3 shows that the $P-T$ dissociation conditions obtained by both methods match very well, indicating that the heating rate chosen for continuous heating was low enough to assume equilibrium conditions for the system at each instant.

Modeling of Gas Hydrate Dissociation Conditions in Pores of Equal Radius. To account for the effect of pore size on hydrate stability, we have used a capillary model based on the extensions of the vdWP model. In the following paragraph, we summarize the vdWP model and deduce the equation involving the pressure, the temperature, and the pore size at gas−water−hydrate equilibrium for a porous medium saturated with water (liquid volume = pore volume).

In the vdWP model, pressure and temperature are uniformly distributed in the bulk phases in contact through planar interfaces. At equilibrium, the chemical potentials of water in the hydrate μ_W^H and water in the liquid phase μ_W^L are equal:

$$\mu_W^H(P,T) = \mu_W^L(P,T) \tag{1}$$

For systems involving a single hydrate former, the chemical potential of water in the hydrate phase can be written in the form based on the vdWP model:

$$\mu_W^H(P,T) = \mu_W^E(P,T) + RT\sum_i \upsilon_i \ln(1-\eta_i) \tag{2}$$

where μ_W^E is the chemical potential of water in a hypothetical empty hydrate lattice, υ_i is the number of type i cavities per water molecule in the hydrate lattice, and η_i is the probability of finding the guest molecule in a cavity of type i and is given by:

$$\eta_i = \frac{C_i f}{1 + C_i f} \tag{3}$$

where f is the fugacity of the hydrate guest in the gaseous state and C_i is the Langmuir adsorption constant. The presence of water vapor in the gas phase was not taken into account. The fugacity was determined using the Peng−Robinson equation

of state[23] (PR-EOS) and C_i was calculated using:

$$C_i = \frac{4\pi}{kT}\int_0^{R_{cell}} \exp\left(-\frac{\omega(r)}{kT}\right) r^2 \, dr \quad (4)$$

where $\omega(r)$ is a spherically symmetric cell potential. The Kihara cell potential with a spherical core was used in the model, and the Kihara parameters were taken from Table 5.3 in the literature.[24]

On the basis of classical thermodynamics, the chemical potential difference of water in the empty hydrate lattice and that in the liquid state can be written as:

$$\frac{\mu_W^E(P,T) - \mu_W^L(P,T)}{RT} = \frac{\Delta\mu_W^0}{RT_0} - \int_{T_0}^{T} \frac{\Delta H_W(T)}{RT^2} dT + \int_0^P \frac{\Delta V_W}{RT} dP - \ln(\gamma_W x_W) \quad (5)$$

where $\Delta\mu_W^0$ is the difference in chemical potentials of water in the empty hydrate lattice, and that, in the pure liquid state for the reference state ($T_0 = 273.15$ K, $P = 0$), ΔH_W and ΔV_W are, respectively, the differences in molar enthalpies and molar volumes of water in the empty hydrate lattice, and that, in the pure liquid state, γ_W is the activity coefficient of water and x_W is the mole fraction of water in the liquid phase.

ΔH_W can be written as:

$$\Delta H_W = \Delta H_W^0 + \int_{T_0}^{T} \Delta C_p \, dT \quad (6)$$

where ΔH_W^0 is the molar enthalpy difference of water in the empty hydrate lattice, and that, in the pure liquid state at 273.15 K, ΔC_p is the molar heat capacity difference. For the temperature dependence of ΔC_p, we used:

$$\Delta C_p = \Delta C_p^0 + b(T - T_0) \quad (7)$$

where ΔC_p^0 is the molar heat capacity difference between the water in the empty hydrate lattice and the liquid state at 273.15 K, and b is a constant.

The activity coefficient of water γ_W was taken equal to unity. The mole fraction of water in the liquid phase x_W was calculated using the correct Henry's law constant expression of Krichevsky and Kasarnovsky:[25]

$$x_W = 1 - x_g = 1 - \frac{f}{h_W \exp\left(\frac{P\bar{V}^\infty}{RT}\right)} \quad (8)$$

where x_g is the mole fraction of gas in the water phase, $\bar{V}^\infty$ is the partial molar volume of gas in water and h_W is the Henry's law constant given by:

$$\ln(h_W) = -(h_W^{(0)}/R + h_W^{(1)}/RT + h_W^{(2)} \ln(T)/R + h_W^{(3)} T/R) \quad (9)$$

with the parameter values being taken from Table 5.3 in the literature.[24]

By combining eqs 1, 2, and 5, the relation between the equilibrium pressure and temperature under which the hydrate dissociates can be written in the form:

$$\frac{\Delta\mu_W^0}{RT_0} - \int_{T_0}^{T} \frac{\Delta H_W(T)}{RT^2} dT + \int_0^P \frac{\Delta V_W}{RT} dP - \sum_i v_i \ln(1 + C_i f) - \ln(\gamma_W x_W) = 0 \quad (10)$$

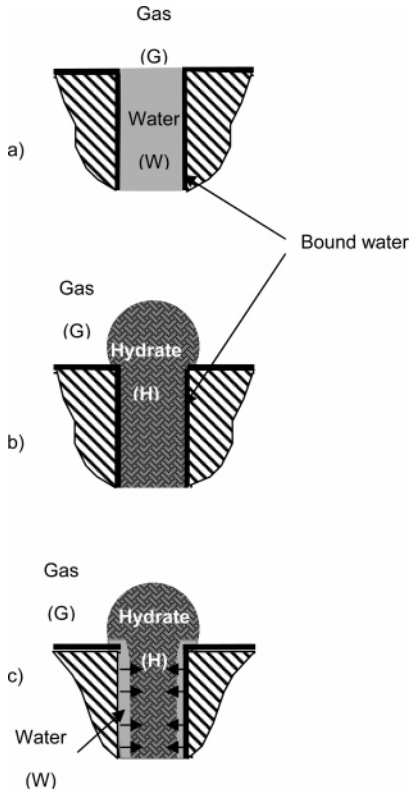

Figure 4. Assumed phase distribution (a) before hydrate formation, (b) after hydrate formation, and (c) during dissociation for porous silica glass saturated with water (liquid volume = pore volume) and for a fractional conversion of water to hydrate (weight of water converted to hydrate/weight of available water) equal to 1.

The left-hand side of eq 10 will be shortened to *BEC* for bulk equilibrium contribution.

When gas hydrates are formed in a porous medium, interfaces (gas−hydrate, hydrate−water, or gas−water) are located inside the pores so that capillary forces contribute to the mechanical balance, and pressure is no longer uniformly distributed between the phases. The chemical potentials of the components in the different phases must include a capillary contribution.

In the present work, we only consider a porous medium initially saturated with water (Figure 4a). If all the water (exclusive of a layer of about 0.4 nm of bound water on pore walls)[15,26] in a pore saturated with water is converted to hydrate, the hydrate phase will protrude outside the pore, due to the fact that the density of hydrate is smaller than that of water (Figure 4b).

Let us consider the pore hydrate in equilibrium with porous water during hydrate dissociation. It is assumed that pore hydrate instantaneously melts along its entire length (Figure 4c). During hydrate dissociation, curved interfaces exist between free gas and bulk hydrate outside the pore and between liquid and pore hydrate inside the pore. When a solid (here, gas hydrate) is in equilibrium with its melt (here, water), it is usually assumed that the contact angle between them is close to 0°. As water is wetting on silica,[27] a thin water film will be present both outside

and inside the pore, and then water can be considered as the continuous phase. Under these conditions, the pressure differences between the phases can be written in the form:[13,16,28]

$$P_H = P_L + F\frac{\sigma_{HW}}{r} \tag{11a}$$

$$P_G = P_L \tag{11b}$$

where P_H, P_L, and P_G are the pressures in the hydrate, liquid, and gas phases, respectively, σ_{HW} is the hydrate−water interfacial tension, r is the pore radius, and F is the shape factor of the hydrate−water interface. During melting, the hydrate−liquid interface has the same shape as that of the pore, and the value of F is usually between 1 and 2.[29,30] For a cylindrical pore, F is 1, whereas for a spherical pore, F is 2. It should be noted that, for hydrate growth, F is 2 because the hydrate−liquid interface is spherical.[14,28,29]

The equilibrium relation for water is written:

$$\mu_W^H(P_H,T) = \mu_W^L(P_L,T) \tag{12}$$

Assuming that the hydrate and liquid phases are incompressible:

$$\mu_W^H(P_H,T) = \mu_W^H(P_G,T) + V_H(P_H - P_G) \tag{13a}$$

$$\mu_W^L(P_L,T) = \mu_W^L(P_G,T) + V_W(P_L - P_G) \tag{13b}$$

where V_H and V_W are the molar volumes of water in the hydrate and liquid states, respectively.

By combining eqs 11a,b, 12, and 13a,b, one obtains:

$$\mu_W^H(P,T) = \mu_W^L(P,T) - F\frac{\sigma_{HW}V_H}{r} \tag{14}$$

where $P = P_G$.

Finally, combining eq 10 and eq 14 gives:

$$BEC = -F\frac{\sigma_{HW}V_H}{rRT} \tag{15}$$

Solving eq 15 will determine the three-phase equilibrium phase boundary for pores of radius r. The right-hand side of eq 15 shifts the equilibrium conditions to lower temperatures and higher pressures when compared with equilibrium conditions for bulk (eq 10). During dissociation of the gas hydrates confined in pores of radius r, the pressure of the three-phase equilibrium will be determined by the temperature and the pore radius. Nevertheless, using eq 15 alone cannot predict the pressure−temperature profile of the hydrate dissociation in pores because it will depend on the CVD of the medium, its saturation state, the fractional conversion of water to hydrate, and the headspace volume. Below, we will demonstrate how, by using eq 15, an equation of state of the gas and the CVD, it is possible to predict the exact dissociation path. We will use this approach to predicting data on hydrate dissociation in pores of varying sizes.

Prediction of the Heating Curve for Gas Hydrate Dissociation in Pores of Different Radii. Let us consider a porous medium with pores of varying sizes saturated with water and known CVD. The initial pressure and temperature in the equilibrium cell, P_A and T_A, must be chosen so that no hydrate is present in the system under these conditions (e.g., point A in Figure 5). The number of moles of CH_4 in the equilibrium cell before hydrate formation, n_{CH4}, is known from the procedure used to charge the cell with the gas. Let us consider the case

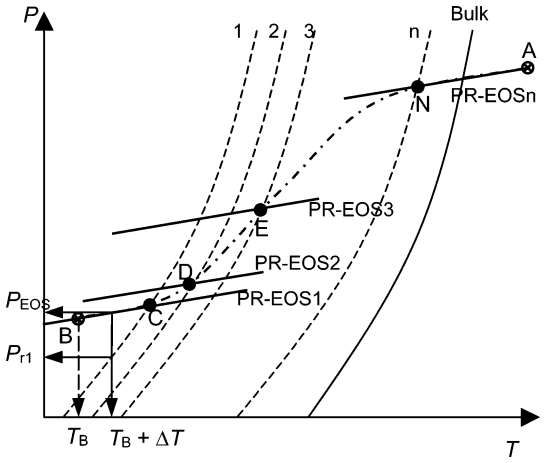

Figure 5. Illustration of the method used to obtain the theoretical heating curve for hydrate dissociation in a porous medium with varying pore sizes. B and A correspond to the conditions before and after hydrate dissociation. The dissociation points C, D, E, and N correspond to the intersections of the equation of state of the gas (PR-EOS curves) and the three-phase equilibrium phase boundary for each pore radius (dotted curves). Between two dissociation points (e.g., D and E), the pressure increase associated with the volume of hydrate that dissociates in pores is calculated from the CVD of the porous medium.

where the fractional conversion of the available water in the pores to hydrate is 1. It is possible to calculate the number of moles of gas consumed in the hydrate formation, and then to deduce the number of moles of gas, n'_{CH4} that remain in the headspace volume. In all the calculus, the reduction/augmentation of the headspace volume due to the hydrate formation/dissociation was taken into account. For methane hydrate composition, we assumed $CH_4 \cdot 6H_2O$. The use of an equation of state (here, the Peng−Robinson equation of state[23] (PR-EOS)) allows calculating the pressure in the gas phase at any temperature (e.g., point B in the curve PR-EOS1 in Figure 5). From the CVD, the smallest pore radius, r_1, is known and eq 15 allows determination of the three-phase equilibrium phase boundary for this pore radius (curve 1 in Figure 5). From the temperature of point B, T_B, the temperature is increased by a temperature step, ΔT. The pressure in the gas phase, P_{EOS}, corresponding to $T = T_B + \Delta T$, is calculated using the PR-EOS and compared to the equilibrium pressure, P_{r1}, calculated from eq 13 at the same temperature. If $|P_{EOS} - P_{r1}|/P_{EOS} > 0.001$, the temperature is incremented and the calculus are reiterated, or else the intersection point of the PR-EOS1 and the three-phase equilibrium phase boundary for pores of radius r_1 (point C in Figure 5) is assumed to be reached. Point C determines the onset of the hydrate dissociation in the porous medium. Once point C has been located in the dissociation curve, the three-phase equilibrium phase boundary for pores of radius r_2 (curve 2 in Figure 5) is determined by using eq 15. The CVD allows calculation of the total volume, V_2, contained by the pores of radius less than or equal to r_2. From V_2, the volume of hydrates in these pores, the number of moles of gas released by the dissociation of these hydrates, Δn_{CH4}, and then the new number of moles of gas in the headspace volume ($n'_{CH4} + \Delta n_{CH4}$) are calculated. The PR-EOS allows calculation of the pressure in the headspace volume at any temperature (curve PR-EOS2 in Figure 5). The intersection point of the PR-EOS2 and the three-phase equilibrium phase boundary for pores of radius r_2 (point D in Figure 5) is searched. Once point D has been located, the variation of total porous volume between the pores of radius r_3 and r_2, $\Delta V = V_3 - V_2$ is calculated using the CVD. The procedure is then repeated to determine the intersec-

TABLE 2: Parameter Values Used in the Model

property	unit	value
$\Delta\mu_W^0$	J/mol	1263[24]
ΔH_W^0	J/mol	−4622[24]
ΔC_p^0	J/(mol K)	−38.12[24]
b	J/(mol K^2)	.141[24]
ΔV_W	m^3/mol	4.6×10^{-6}
σ_{HW}	J/m^2	.032[15]
$\bar{V}^\infty$	m^3/mol	34.7×10^{-6} [31]
V_W	m^3/mol	18.02×10^{-6}
Critical Properties of CH_4 (Obtained from the DIPPR Database) Used in the PR-EOS		
critical temperature	K	190.6
critical pressure	kPa	4599
acentric factor		.0115

tion point of the PR-EOS3 and the three-phase equilibrium phase boundary for pores of radius r_3 (point E in Figure 5). Applying this method until the pore of maximum radius r_m is reached and then joining all the dissociation points allows obtaining of the predicted heating curve for methane hydrate dissociation in the porous medium.

Results and Discussions

The $P-T$ dissociation conditions of methane hydrates confined in the CPG sample were first measured for the range of pressure 10−20 MPa. In this experiment, the number of moles of CH_4 introduced in the equilibrium cell was about 1.83. The pressure and temperature in the gas phase, used as P_A and T_A in the aforementioned method, before the hydrate formation/dissociation cycle were 18.6 MPa and 294 K, respectively. The amount of available water was calculated as the weight of liquid water added to the CPG sample plus the weight of the residual adsorbed water (3.05 wt % of the sample) minus the weight of surface-bound water contained in a layer of 0.4 nm on the pore walls. As one might expect, the amount of available water roughly corresponds to the weight of liquid water added to dry silica (e.g., 40 g of liquid water added to 41.6 g of dry silica gives 39.8 g of available water).

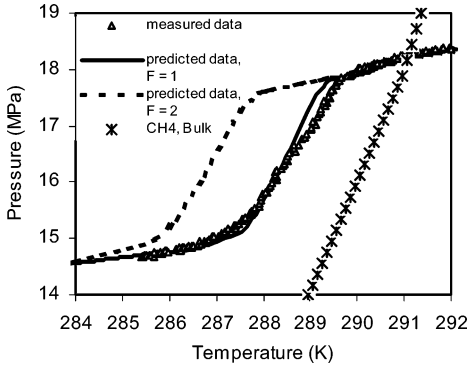

Figure 6. Experimental and theoretical heating curves for methane hydrate dissociation in porous silica glass. $F = 1$ (solid line) corresponds to a cylindrical shape for the hydrate particles. $F = 2$ (dotted line) corresponds to a spherical shape for the hydrate particles.

The predicted heating curves for methane hydrate dissociation in the CPG sample, obtained using our approach with the parameter values given in Table 2, are shown in Figure 6 and compared to the measured data. The fractional conversion of available water to hydrate was assumed to be 1. The solid line in Figure 6 represents the predictions using a shape factor (F) of 1, i.e., assuming a cylindrical contact between the hydrate and aqueous phase in pores during hydrate dissociation. The predicted dissociation pattern closely resembles that measured, supporting the validity of the method. Moreover, the predicted equilibrium pressures are very good, with a maximum relative deviation ($|P_{pred} - P_{exp}|/P_{exp}$) of 2.3% (Table 3). The good agreement between the predicted and measured heating curves for the low pressures and temperatures confirms that all the available water was converted to hydrate. The dotted line in Figure 6 corresponds to the predicted curve using $F = 2$. In this case, the hydrate−water interface is assumed to be spherical,

TABLE 3: Comparison of Experimental and Predicted Dissociation Pressures

T (K)	P_{exp}[a] (MPa)	P_{pred}[a] (MPa)	relative deviation[a] (%)	P_{exp}[b] (MPa)	P_{pred}[b] (MPa)	relative deviation[b] (%)	P_{pred}[b,c] (MPa)	relative deviation[b,c] (%)
285.4	14.67	14.70	0.22					
285.7	14.71	14.73	0.14					
286.0	14.77	14.76	0.07					
286.4	14.85	14.79	0.37					
286.8	14.93	14.88	0.35					
287.0	15.02	14.95	0.47					
287.3	15.11	15.04	0.46					
287.7	15.37	15.20	1.13					
288.1	15.81	15.80	0.06					
288.4	16.28	16.32	0.24	22.38	22.45	0.31		
288.7	16.55	16.80	1.51	22.42	22.50	0.35		
289.0	16.94	17.33	2.30	22.48	22.55	0.31	17.42	22.51
289.3	17.44	17.74	1.73	22.57	22.60	0.13	18.12	19.72
289.6	17.77	17.84	0.39	22.64	22.64	0.01	18.85	16.73
289.9	17.92	17.88	0.23	22.74	22.73	0.04	19.63	13.68
290.1	18.02	17.92	0.66	22.86	22.82	0.15	20.15	11.85
290.3	18.04	17.95	0.41	22.95	22.87	0.33	20.70	9.79
290.6	18.13	18.17	0.24	23.06	23.00	0.26	21.54	6.59
290.9	18.24	18.19	0.28	23.40	23.18	0.92	22.43	4.15
291.2	18.29	18.23	0.30	23.82	23.82	0.00	23.34	2.03
291.5	18.30	18.27	0.16	24.48	24.58	0.37	24.3	0.75
291.8	18.35	18.31	0.19	25.11	25.32	0.84	25.32	0.84
292.1	18.42	18.35	0.37	25.64	25.96	1.24	26.37	2.85
292.4	18.45	18.39	0.31	26.23	26.42	0.72	27.45	4.65
292.7	18.48	18.43	0.26	26.46	26.49	0.09	28.60	8.08
293.0	18.50	18.46	0.22	26.58	26.55	0.10	29.70	11.74

[a] Data from Figure 6; predicted pressures obtained with $F = 1$. [b] Data from Figure 7. [c] Predicted pressures obtained with eq 15 for the mean (or nominal) pore radius $r_{mean} = (32-0.8)/2$.

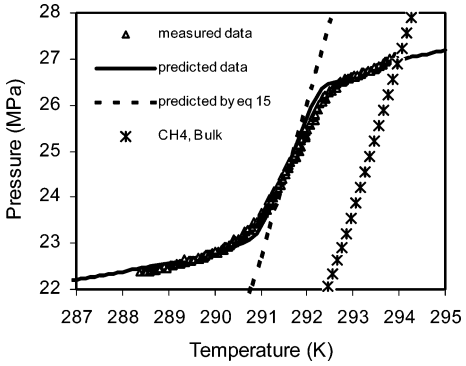

Figure 7. Experimental and theoretical heating curves for methane hydrate dissociation in porous silica glass for higher pressures than in Figure 6 and for $F = 1$. The dotted line corresponds to the three-phase equilibrium phase boundary calculated with eq 15 for the mean pore radius $r_{mean} = (32-0.8)/2$.

which should correspond to hydrate dissociation in spherical pores. The fact that predictions with $F = 1$ are much better than those obtained with $F = 2$ means that the shape of melting hydrate particles confined in the pores of the studied CPG sample was rather cylindrical.

To check once again the validity of the method, we investigated the dissociation conditions of methane hydrate in the same porous medium but for a pressure range of 20−30 MPa. In this new experiment, the number of moles of CH_4 introduced in the equilibrium cell was about 2.49, and P_A and T_A were 27.6 MPa and 296 K, respectively. The predicted heating curve obtained for $F = 1$ is shown in Figure 7 and compared to the measured data. The agreement between the prediction and the experimental data seems very good, with a maximum relative deviation of about 1.3% (Table 3).

We also plotted in Figure 7 the three-phase equilibrium phase boundary (dotted line) calculated with eq 15 for the mean pore radius $r_{mean} = (32-0.8)/2$ (where 0.8 is twice the thickness of the layer of bound water) and $F = 1$. Table 3 clearly shows that much more reliable predictions are obtained when the PSD of the porous medium rather than the size corresponding to the pores of dominant porosity is taken into account.

Conclusions

By considering the cumulative volume distribution (CVD) of the porous medium, and using both an extension of the vdWP model that includes a capillary term and an equation of state of the gas, we have shown that it is possible to reproduce, for isochoric conditions, the experimental heating curves for gas hydrate dissociation in a porous silica glass, which was initially saturated with water, and for a fractional conversion of available water to hydrate of 1. This work confirms that the heating curves closely reflect the CVD of the porous medium. The shape factor F was found equal to 1, which supports a cylindrical shape for hydrate particles dissociating in the pores of silica glass.

The proposed method allows more correct interpretations of the heating curve data obtained for fixed-volume laboratory systems and gives excellent predictions for different ranges of pressure and temperature.

Further studies need to be performed to further test this method and, more specifically, the model used in the method. For example, the method could be applied for undersaturated systems (pore volume > liquid volume) and/or for fractional conversion of water to hydrate different from 1. For undersaturated systems, where gas intrudes into pores, the added effect of the curvature of the solid−gas interface on phase pressures should be taken into account in the capillary term. For fractional conversions of water to hydrate smaller than 1, the smallest pores are filled by water not hydrate, and the method could be used to determine the size of the smallest pores containing hydrates by comparing heating curve charts obtained by varying the fractional conversion of water to hydrate with the measured heating curve.

Acknowledgment. This work was supported financially by Total. The authors wish to thank Dr. François Fajula, UMR 5618 CNRS-ENSCM-UMI, for help with the nitrogen adsorption/desorption measurements of the studied CPG sample.

References and Notes

(1) Turner, D.; Sloan, E. D. Hydrate Phase Equilibria Measurements and Predictions in Sediments. In *Proceedings of the Fourth International Conference on Gas Hydrates*, Yokohama, Japan, May 19−23, 2002.

(2) Chuvilin, E. M.; Kozlova, E. V.; Makhonina, N. A.; Yakushev, V. S.; Dubinyak, D. V. Peculiarities of Methane Hydrate Formation/Dissociation P/T Conditions in Sediments of Different Composition. In *Proceedings of the Fourth International Conference on Gas Hydrates*, Yokohama, Japan, May 19−23, 2002.

(3) Handa, Y. P.; Stupin, D. *J. Phys. Chem.* **1992**, *96*, 8599.

(4) Melnikov, V. P.; Nesterov, A. N. Modelling of Gas Hydrates Formation in Porous Media. In *Proceedings of the Second International Conference on Gas Hydrates*, Toulouse, France, June 2−6, 1996.

(5) Clennell, M. B.; Hovland, M.; Booth, J. S.; Henry, P.; Winters, W. J. *J. Geophys. Res.* **1999**, *104*, 22985.

(6) Uchida, T.; Ebinuma, T.; Ishizaki, T. *J. Phys. Chem. B* **1999**, *103*, 3659.

(7) Uchida, T.; Ebinuma, T.; Takeya, S.; Nagao, J.; Narita, H. *J. Phys. Chem. B* **2002**, *106*, 820.

(8) Buffet, B. A.; Zatsepina, O. Y. *Mar. Geol.* **2000**, *164*, 69.

(9) Wilder, J. W.; Seshadri, K.; Smith D. H. *Langmuir* **2001**, *17*, 6729.

(10) Wilder, J. W.; Seshadri, K.; Smith D. H. *J. Phys. Chem B* **2001**, *105*, 9970.

(11) Zhang, W.; Wilder, J. W.; Smith D. H. *J. Phys. Chem. B* **2003**, *107*, 13084.

(12) Klauda, J. B.; Sandler, S. I. *Ind. Eng. Chem. Res.* **2001**, *40*, 4197.

(13) Klauda, J. B.; Sandler, S. I. *Mar. Pet. Geol.* **2003**, *20*, 459.

(14) Anderson, R.; Llamedo, M.; Tohidi, B.; Burgass, R. W. *J. Phys. Chem. B* **2003**, *107*, 3500.

(15) Anderson, R.; Llamedo, M.; Tohidi, B.; Burgass, R. W. *J. Phys. Chem. B* **2003**, *107*, 3507.

(16) Østergaard, K. K.; Anderson, R.; Llamedo, M.; Tohidi, B. *Terra Nova* **2002**, *14*, 307.

(17) Melnikov, V. P.; Nesterov, A. N. *Earth Cryosphere* **2001**, *5*, 3.

(18) Henry, P.; Thomas, M.; Clennell, B. *J. Geophys. Res.* **1999**, *104*, 23005.

(19) Clarke, M. A.; Pooladi-Darvish, M.; Bishnoi, P. R. *Ind. Eng. Chem. Res.* **1999**, *38*, 2485.

(20) Barrett, E. P.; Joyner, L. G.; Halenda, P. H. *J. Am. Chem. Soc.* **1951**, *73*, 373.

(21) Brunauer, S.; Emmett, P. H.; Teller, E. *J. Am. Chem. Soc.* **1938**, *60*, 309.

(22) Tohidi, B.; Burgass, R. W.; Danesh, A.; Østergaard, K. K.; Todd, A. C. *Ann. N.Y. Acad. Sci.* **2000**, *912*, 924.

(23) Peng, D.; Robinson, D. B. *Ind. Eng. Chem. Fundam.* **1976**, *15*, 59.

(24) Sloan, E. D. *Clathrate Hydrates of Natural Gases*, 2nd ed.; Marcel Dekker: New York, 1997.

(25) Krichevsky, I. R.; Kasarnovsky, J. S. *J. Am. Chem. Soc.* **1935**, *60*, 309.

(26) Schreiber, A.; Ketelsen, I.; Findenegg, G. H. *Phys. Chem. Chem. Phys.* **2001**, *3*, 1185.

(27) Tohidi, B.; Anderson, R.; Clennell, B.; Burgass, R. W.; Biderkab, A. B. *Geology* **2001**, *29*, 867.

(28) Llamedo, M.; Anderson, R.; Tohidi, B. *Am. Mineral.* **2004**, *89*, 1264.

(29) Handa, Y. P.; Zakrzewski, M.; Fairbridge, C. *J. Phys. Chem.* **1992**, *96*, 8594.

(30) Aladko, E. Ya.; Dyadin, Y. A.; Fenelonov, V. B.; Larionov, E. G.; Mel'gunov, M. S.; Manakov, A. Yu.; Nesterov, A. N.; Zhurko, F. V. *J. Phys. Chem. B* **2004**, *108*, 16540.

(31) Handa, Y. P. *J. Phys. Chem.* **1990**, *94*, 2652.